



# Two-dimensional PtSe<sub>2</sub> Theoretically Enhanced Goos-Hänchen Shift Sensitive Plasmonic Biosensors

Yan Guo<sup>1,2</sup> · Nishtha Manish Singh<sup>3</sup> · Chandreyee Manas Das<sup>2,3</sup> · Qingling Ouyang<sup>2,3</sup> · Lixing Kang<sup>2,3</sup> · Kuanbiao Li<sup>4</sup> · Philippe Coquet<sup>2,5</sup> · Ken-Tye Yong<sup>2,3</sup>

Received: 18 March 2020 / Accepted: 27 May 2020 / Published online: 6 June 2020  
© Springer Science+Business Media, LLC, part of Springer Nature 2020

## Abstract

Platinum diselenide (PtSe<sub>2</sub>), an emerging two-dimensional transition metal dichalcogenide, exhibits thickness-dependent refractive index, and hence, intriguing optical properties. Here, we employ it as a plasmonic sensing substrate to achieve significant enhancement in Goos-Hänchen shift sensitivity. Through systematic optimization of all parameters, four optimum sensing configurations have been achieved at different wavelengths ranging from visible to near-infrared region, where the Goos-Hänchen shift sensitivity receives four times enhancement in comparison with the conventional bare gold sensing substrate. There is a linear range of Goos-Hänchen shift with the tiny change of refractive index for each optimal configuration. The detection limit of the refractive index change can be as low as  $5 \times 10^{-7}$  RIU which is estimated to be lower by 2 orders of magnitude, and the corresponding sensitivity of biomolecules has a 1000-fold increment compared with that of bare gold-based sensors.

**Keywords** Surface plasmon resonance · Plasmonic biosensor · Goos-Hänchen shift · Sensitivity · Platinum diselenide

## Introduction

The Goos-Hänchen (GH) effect is a phenomenon of geometric optics where the light beam, reflected from the interface of

dielectric media, shifts laterally in the plane of incidence away from the theoretically predicted position [1]. This kind of shift is called GH shift. After the innovation of laser and the development of integral optics, the GH shift phenomenon has been actively explored for applications in electronics [2, 3], optical waveguide switch [4], and optical temperature sensing [5]. The stationary phase method, proposed by Artmann, theoretically explains this effect and clearly indicates its close relationship with the phase change of the reflected light [6]. Surface plasmon resonance (SPR) is a special electromagnetic wave resulting from the surface charge density collective oscillation, which is excited at the interface between two materials having negative and positive permittivities, respectively. And the SPR has been extensively studied in theory and experiment and used in the development of biosensors for medical diagnostics [7], food safety, and other areas. In the SPR arrangement, an abrupt change in the phase of a *p*-polarized (whose polarization direction is parallel to the incident plane) reflected light occurs at the resonance condition. Hence, the SPR effect has been widely investigated in the plasmonic sensing field to detect chemical and biological parameters that cause the change in refractive index (RI) near the sensing interface [8, 9]. Thus, it is natural to propose the combination of the GH shift effect and SPR sensing through phase change measurements occurring at the minimum reflectivity point of the SPR curve [10–13].

**Electronic supplementary material** The online version of this article (<https://doi.org/10.1007/s11468-020-01204-9>) contains supplementary material, which is available to authorized users.

✉ Yan Guo  
guoyan@hdu.edu.cn

✉ Ken-Tye Yong  
ktyong@ntu.edu.sg

<sup>1</sup> School of Automation, Hangzhou Dianzi University, Hangzhou 310018, Zhejiang, China

<sup>2</sup> CINTRA CNRS/NTU/THALES, UMI 3288, Research Techno Plaza, 50 Nanyang Drive, Border X Block, Singapore 637553, Singapore

<sup>3</sup> School of Electrical and Electronic Engineering, Nanyang Technological University, 50 Nanyang Avenue, Singapore 639798, Singapore

<sup>4</sup> HANGZHOU HANGYANG Co. Ltd, Hangzhou 310014, Zhejiang, China

<sup>5</sup> Institut d'Electronique, de Microélectronique et de Nanotechnologie (IEMN), CNRS UMR 8520 -Université de Lille 1, 59650 Villeneuve d'Ascq, France

Two-dimensional (2D) transition metal dichalcogenides (TMDCs) are gathering rising research interest because of their unique properties such as tunable photonic bandgap, high charge mobility, and large absorption of light [14, 15]. Specifically, PtSe<sub>2</sub>, an emerging group 10 TMDC, bears optical properties different from other group 6 TMDCs. It has a 1T-phase, implying 6 Se atoms in the space surround one Pt atom, as seen from the top view. The continuous 1T-PtSe<sub>2</sub> is an isotropic plane, and its monolayer film with the thickness of 2.53 Å can provide the biggest bandgap of 1.2 eV [16]. In contrast, bilayer PtSe<sub>2</sub> samples with interlayer distance of 5.07 Å have a narrower bandgap of 0.21 eV. The interlayer distance between multiple layers or bulk PtSe<sub>2</sub> reduces on increasing the layer numbers because of the strong coupling covalent bands between the neighboring structure. Hence, PtSe<sub>2</sub> undergoes a phase transition from the indirect bandgap semiconductor of the monolayer and bilayer structures to a semimetal character of multiple layers and bulk PtSe<sub>2</sub> [17, 18]. The RI of this layer-dependent material as well as its absorption spectrum also depends strongly on the film thickness [19], which provides another modulation method when the material is applied to optoelectronic devices [16, 20]. In addition, PtSe<sub>2</sub> has extremely high mobility of 3000 cm<sup>2</sup> V<sup>-1</sup> s<sup>-1</sup>, and large electrical conductivity which can only be achieved by varying its thickness [21–23]. These characteristics of PtSe<sub>2</sub> allow it to be an ideal candidate for high-speed electronic applications in the infrared region. However, controlled preparation of this 2D TMDC material with large-area and high-quality uniform is still a huge challenge, so it is of critical advantages to investigate the characteristics of this material in theory and provide certain guided advice when the sound preparation process is developed.

In the present work, we systemically design and simulate the plasmonic sensing schemes at conditions of (1) different PtSe<sub>2</sub> thicknesses, (2) discrete excitation wavelengths, and (3) different types of coupling prism, to improve the sensitivity of biomolecular GH shift sensor based on SPR configuration. We also consider the assistant role of graphene on improving the sensing performance based on the high optical absorption rate of graphene and wavelength-dependent RI variation tendency similar to that of PtSe<sub>2</sub>. By tuning (a) the gold film's thickness, (b) the layer numbers of graphene, and (c) the thickness of PtSe<sub>2</sub> layer, four optimum sensing configurations can be found at different excitation wavelengths. One of these configurations shows a GH shift sensitivity enhancement of four times more than that of sensors based on bare gold. In addition, we also report the detection limit for solutions containing low concentrations of biomolecules and the corresponding sensitivity with the optimum sensing configurations.

## Theory and Simulation Method

In the present simulation, we employ four different wavelengths (532 nm, 632.8 nm, 780 nm, and 1152 nm) spanning

from visible light to near-infrared region. They are the working wavelengths irradiated by Nd:YAG laser or diode pump solid-state laser (532 nm), He-Ne gas laser (632.8 nm, 1152 nm), and GaAlAs laser (780 nm), all of which are widely used in the laboratory and industry. Additionally, three different prisms, namely BK7, SF5, and SF11, most commonly applied in the SPR configurations, are chosen to couple the incident light into the proposed biosensor. Titanium (Ti) layer with 2.5 nm thickness is utilized to attach gold (Au) onto the prism. While gold and silver are usually chosen to be the plasmonic metal of SPR-based sensors, gold is preferred because of its chemical stability. Since a too thin or too thick gold film is not good at coupling electromagnetic waves into surface waves, the thickness of gold film is increased from 30 nm by 1-nm step to 60 nm. Graphene dielectric layers with excellent optoelectronic properties are grown on the upper surface of gold thin film to improve the SPR biosensor sensitivity. The thickness of monolayer graphene is 0.34 nm, so the total thickness of *L*-layer graphene equals to  $d = L \times 0.34$  nm [24]. 2D PtSe<sub>2</sub> with different thicknesses is coated over graphene, and it acts as the sensing interface which contacts directly with the sensing medium. The incident angle is adjusted from the critical angle to the almost grazing incidence by the spacing of 0.1° which is reasonable according to the precision accuracies of the rotation stage and micrometer used in the experiment. At first, we consider de-ionized (DI) water to be the analyte solution, and later, DI water contains biomolecules. The RI of analyte solution will increase by  $\Delta n_{\text{bio}}$  after biomolecules are adsorbed on the PtSe<sub>2</sub> surface. Briefly, this is a six-layered system, containing the prism, titanium, gold, graphene, PtSe<sub>2</sub>, and analyte solution, as shown in Fig. 1. The refractive indices of all these materials at the four excitation wavelengths are presented in Table 1.

Since only *p*-polarized lights can excite the surface plasmons, the *s*-polarized lights (whose polarization direction is perpendicular to the incident plane) can be used as a reference to determine other parameters' influence on the sensing performance. This is an advantageous factor as it aids not only in eliminating the environmental noises but also in reducing the error caused by the non-ideal profile of the light source when doing experiments to improve the measurement accuracy.

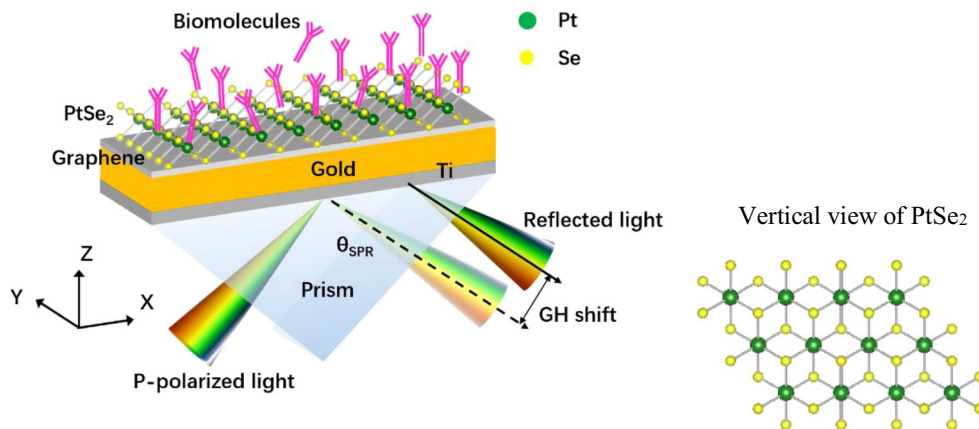
Coming to the principle behind the GH shift, for one interface system, when a beam illuminates from dielectric 1 with permittivity of  $\varepsilon_1$  onto the interface of dielectric 2 with permittivity of  $\varepsilon_2$  at an incident angle of  $\theta$ , the reflectivity equals to

$$r_p(\theta, \omega) = \left( \frac{k_{z1} - k_{z2}}{\varepsilon_1 - \varepsilon_2} \right) / \left( \frac{k_{z1} + k_{z2}}{\varepsilon_1 + \varepsilon_2} \right) \quad (1)$$

for the *p*-polarized light and

$$r_s(\theta, \omega) = (k_{z1} - k_{z2}) / (k_{z1} + k_{z2}) \quad (2)$$

**Fig. 1** *P*-polarized reflected light from the layered sensing system of graphene-assisted 2D PtSe<sub>2</sub> to enhance GH lateral shift. The inset is the vertical view of PtSe<sub>2</sub>



for the *s*-polarized light, where  $k_{z1} = \omega/c\sqrt{\epsilon_1}\cos\theta$  and  $k_{z2} = \omega/c\sqrt{\epsilon_2-\epsilon_1\sin^2\theta}$ .

But for an *N*-layered model presented here, we need to employ the transfer matrix method (TMM) to achieve the systemic reflectivity coefficient [28]. The matrix of the *N*-layered model is defined as

$$M = \prod_{k=2}^{N-1} M_k = \begin{bmatrix} M_{11} & M_{12} \\ M_{21} & M_{22} \end{bmatrix} \tag{3}$$

where  $M_k$  indicates the matrix of the *k*th layer. For *p*-polarized incident lights,  $M_k$  can be given by

$$M_k = \begin{bmatrix} \cos\beta_k & -i\sin\beta_k/q_k \\ -iq_k\sin\beta_k & \cos\beta_k \end{bmatrix} \tag{4}$$

where  $q_k = \frac{(\epsilon_k - n_1^2 \sin^2 \theta_1)^{1/2}}{\epsilon_k} = \frac{\lambda \beta_k}{2\pi d_k \epsilon_k}$ ,  $\beta_k = \frac{2\pi d_k}{\lambda} (\epsilon_k - n_1^2 \sin^2 \theta_1)^{1/2}$ , and  $d_k$  is the thickness of the *k*th layer. Hence, it can easily obtain the four elements of the matrix— $M_{11}$ ,  $M_{12}$ ,  $M_{21}$ , and  $M_{22}$ . Then, considering the boundary conditions of the electromagnetic wave propagation, the amplitude reflectivity coefficient  $r_p$  of the *N*-layered model is obtained by

$$r_p = \frac{(M_{11} + M_{12}q_N)q_1 - (M_{21} + M_{22}q_N)}{(M_{11} + M_{12}q_N)q_1 + (M_{21} + M_{22}q_N)} \tag{5}$$

which is a complex quantity and can be written as  $r_p = |r_p|e^{i\phi_p}$ . Thus, the reflectivity  $R_p$  and phase  $\phi_p$  of the *p*-polarized light are respectively extracted by

$$R_p = |r_p|^2 \text{ and } \phi_p = \arg(r_p) \tag{6}$$

The GH shift is obtained by differentiating phase as a function of the incident angle according to the stationary phase theory:

$$\text{GHs}_p = -\frac{\lambda}{2\pi} \frac{d\phi_p}{d\theta} \tag{7}$$

For *s*-polarized incident lights, the same equations hold, with  $q_k$  replaced by  $p_k = (\epsilon_k - n_1^2 \sin^2 \theta_1)^{1/2}$ . So, the differential GH shift between *s*- and *p*-polarized lights is  $\text{GHs} = \text{GHs}_p - \text{GHs}_s$ . The GH shift sensitivity *S* is then referred to be the ratio of the differential GH shift change  $\Delta\text{GHs} = \text{GHs}|_{n+\Delta n_{\text{bio}}} - \text{GHs}|_n$  to the RI change  $\Delta n_{\text{bio}}$  of the sensing medium caused by biomolecular adsorption, i.e.,

**Table 1** Refractive indices (RI) of Au, prisms (BK7/SF5/SF11), graphene, DI water, titanium, and PtSe<sub>2</sub> with different thicknesses at various excitation wavelengths used in the proposed structure

RI	$\lambda = 532 \text{ nm}$	$\lambda = 632.8 \text{ nm}$	$\lambda = 780 \text{ nm}$	$\lambda = 1152 \text{ nm}$
Au [25]	0.0990 + i2.9952	0.1377 + i3.6183	0.2063 + i4.5133	0.4417 + i6.7308
BK7 [26]	1.5195	1.5151	1.5112	1.5055
SF5	1.6796	1.6685	1.6595	1.6489
SF11	1.7948	1.7786	1.7658	1.7515
Graphene [24]	3 + i0.9658	3 + i1.1487	3 + i1.4160	3 + i2.0913
DI water [26]	1.3369	1.3326	1.3264	1.3189
Ti [27]	2.4793 + i3.3511	2.7039 + i3.7651	3.0775 + i4.01	3.5600 + i4.0850
PtSe <sub>2</sub> 2 nm [19]	2.5917 + i1.1332	2.9029 + i0.8905	2.8229 + i0.5277	2.7986 + i0.2878
PtSe <sub>2</sub> 4 nm	2.5002 + i1.3835	2.9161 + i1.2986	3.3009 + i0.9076	3.2582 + i0.3881
PtSe <sub>2</sub> 6 nm	2.6762 + i1.6724	3.0168 + i1.6734	3.5912 + i1.5030	3.7622 + i0.6462

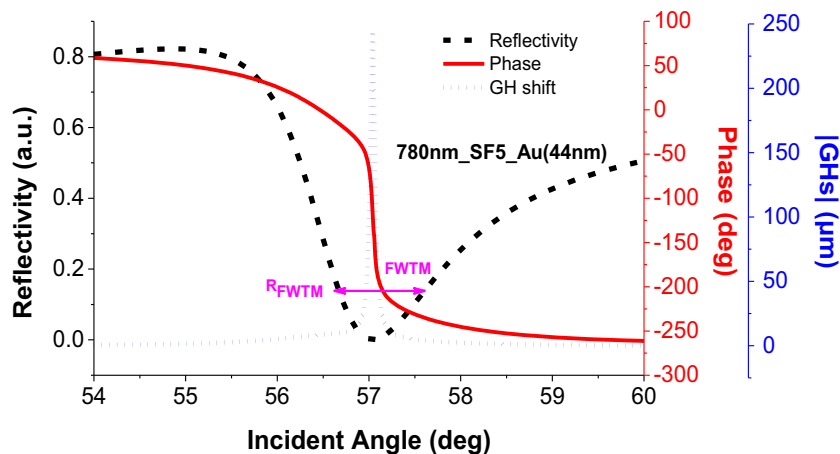
$$S = \frac{|\Delta GHs|}{\Delta n_{bio}} \quad (8)$$

Here, the detection accuracy of the GH shift sensing system is defined to be the full width at one-tenth maximum (FWTM) to characterize the sensing performance. The corresponding reflectivity  $R_{FWTM}$  at one-tenth maximum equals to  $R_{FWTM} = 0.1 \times (R_{max} + 9R_{min})$ , wherein  $R_{max}$  and  $R_{min}$  representing the maximum and minimum reflectivities, respectively. The smaller the FWTM, the higher the detection accuracy. The sensing substrate and the optical parameters of all the underlying layers determine the value of FWTM. Enhanced factor refers to the ratio of sensitivity of the optimum sensing models to that of conventional bare gold sensing system, which quantitatively characterizes the enhancement sensitivity in the sensing models.

## Results and Discussion

Before systematically investigating the GH shift sensitivity with these layered substrates in the sensing model, it is better to validate the relationship between the SPR excitation, phase abruption, and GH shift. If not specified in the following description, reflectivity refers to the reflectivity of  $p$ -polarized light. Since the SPR excitation leads to a drastic change in phase, the largest GH shift can be obtained. Figure 2 presents the complementary relationship between the minimum reflectivity of SPR curve, phase abruption, and the corresponding GH shift. For a thorough investigation of the influence of graphene and PtSe<sub>2</sub> on the conventional SPR-based biomolecular sensor, we design three comparison models. In this paper, the conventional sensor structure with bare gold thin film is referred to be the first model. The second model is obtained by adding a layer of PtSe<sub>2</sub> on the gold layer. The third model covers  $L$  layers of graphene between the gold film and PtSe<sub>2</sub>.

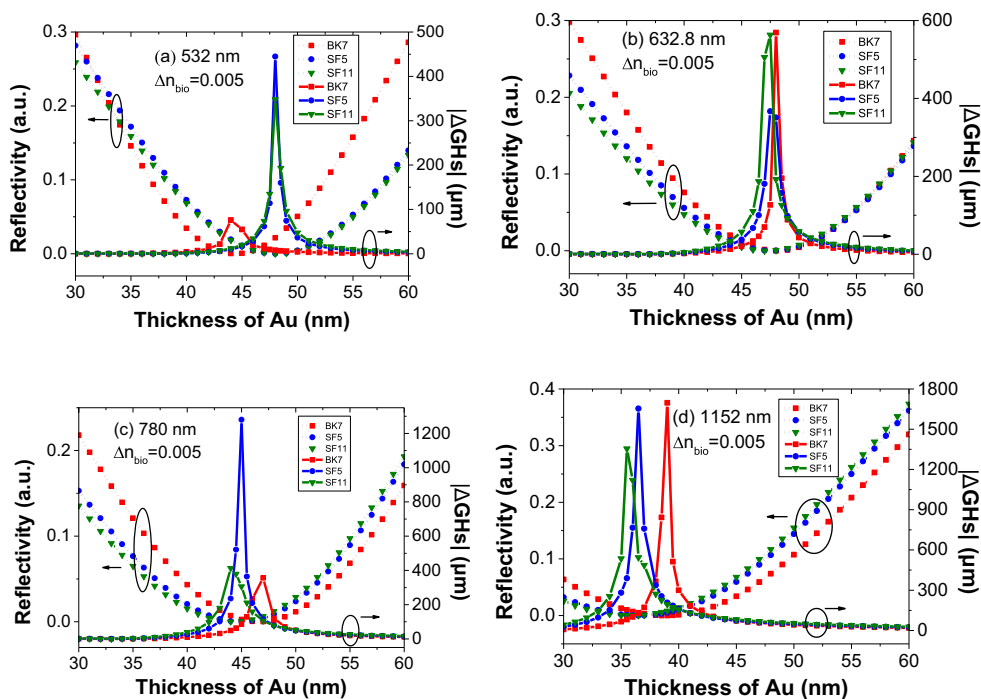
**Fig. 2** Reflectivity (dash), phase (solid), and GH shift (dotted) curves for the  $p$ -polarized light with respect to the incident angle for bare gold substrate coupled by SF5 prism at the excitation wavelength of 780 nm. The maximum GH shift and the most dramatic phase change coincide very well at the SPR angle. The FWTM of the reflectivity curve at  $R_{FWTM}$  denoted in pink equals to 0.68°



In the simulation, the gold film's thickness is increased from 30 nm by a 1-nm step to 60 nm. The comparison details between the SPR curves, phase changes, and GH shifts with various parameters are shown in Fig. S1. The minimum reflectivity of the SPR curve for every gold thickness can be obtained with different excitation wavelengths and coupling prisms, and the data are summarized in Fig. 3 (dotted curves). For each case, there exists an optimum gold thickness to achieve the maximum energy transfer and the minimum reflectivity. But the optimum gold thickness is different for each type of coupling prism. This is because the wavevector of SPR differs with the coupling prism according to the wavevector matching condition. In addition, the thickness of gold thin film plays a crucial role in exciting SPR because it can affect the coupling intensity of SPRs on both sides of the film. Hence, the optimum gold thickness depends on the applied wavelength and prism. Moreover, the optimum gold thickness decreases when the incident wavelength increases resulting from the increment of complex RI of gold. The solid curves in Fig. 3 are the counterpart modular changes of differential GH shift  $|\Delta GHs|$  with the RI change of  $\Delta n_{bio} = 0.005$ . It is clear that the maximum modular change of differential GH shift is coincident with its reflectivity curve. The lower the reflectivity, the larger the modular change of differential GH shift  $|\Delta GHs|$ . In addition, a special prism utilized to couple a given incident light can yield the largest sensing signal.

The SPR curves for the second model at different thicknesses of PtSe<sub>2</sub> and other parameters are shown in Fig. 4a. When all parameters of the whole system achieves optimum values, the minimum reflectivity can reach  $10^{-5}$ . Even though the gold-excited SPR is mainly in the visible region, the near-infrared wavelength of 1152 nm can also effectively excite SPR due to the high electron mobility provided by PtSe<sub>2</sub>. The incident light wavelength not only changes the SPR angle through affecting its wavevector but also affects the width of SPR curve. The long excitation wavelength utilized has an appreciable effect on the width of the resonance curve which is determined by the complex permittivity of the metal.

**Fig. 3** Minimum reflectivities with respect to the gold thickness (dotted curves) for different coupling prisms at the excitation wavelengths of **a** 532 nm, **b** 632.8 nm, **c** 780 nm, and **d** 1152 nm; solid lines in every pattern represent the corresponding modular changes in differential GH shift  $|\Delta GHs|$  with the refractive index change of  $\Delta n_{\text{bio}} = 0.005$  for the first model



Generally, a complex permittivity having a big real part, together with a small imaginary part, results in narrow resonance curves. It is observed that the influence of PtSe<sub>2</sub> thickness mainly determines the width of the SPR curve because of its layer dependence of refractive index, while it has small

impact on the SPR excitation efficiency since not much difference between the minimal reflectivities of the two blue curves (excitation wavelength of 780 nm). In addition, the SPR curve becomes even narrower with long waves because the imaginary part of the refractive index of PtSe<sub>2</sub> reduces

**Fig. 4** **a** SPR curves and **b** the corresponding GH shift lines with DI water as the analyte solution for different parameter combinations (presenting in legends) for the second model

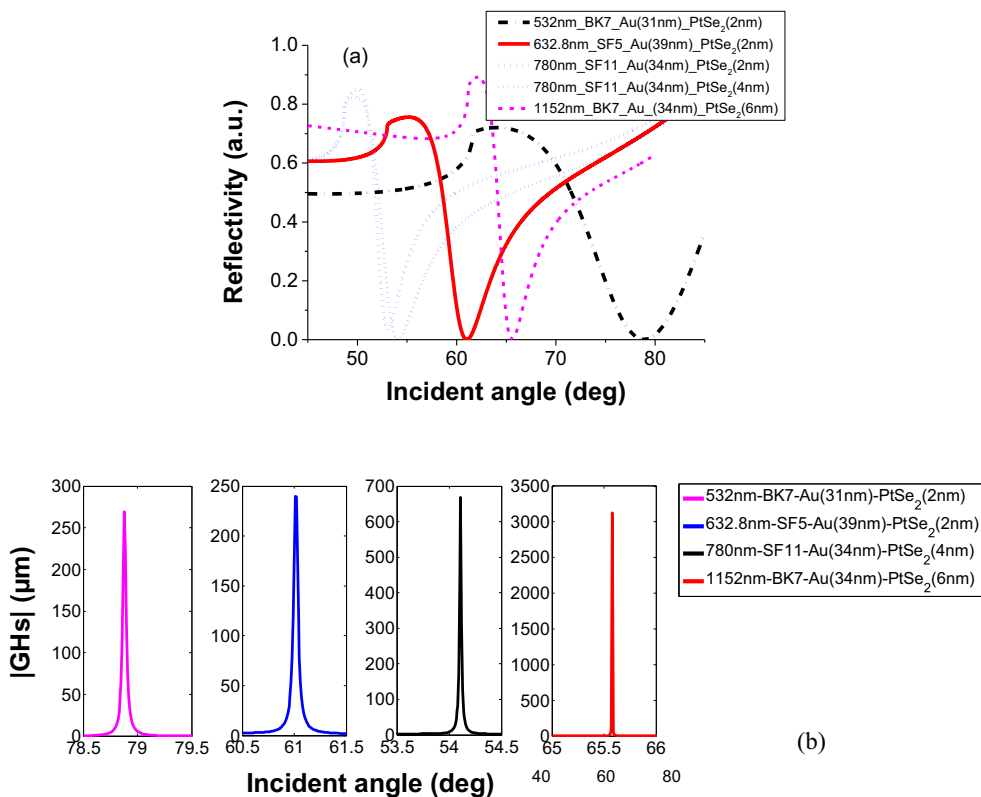


**Fig. 5** The modular of differential GH shift  $|\Delta\text{GHs}|$  with respect to the thickness of gold thin film and prisms with PtSe<sub>2</sub> thickness of 2 nm at excitation wavelengths of **a** 532 nm, **b** 632.8 nm, **c** 780 nm, and **d** 1152 nm when the RI change of the aqueous solution equals to  $\Delta n_{\text{bio}} = 0.005$  for the second model

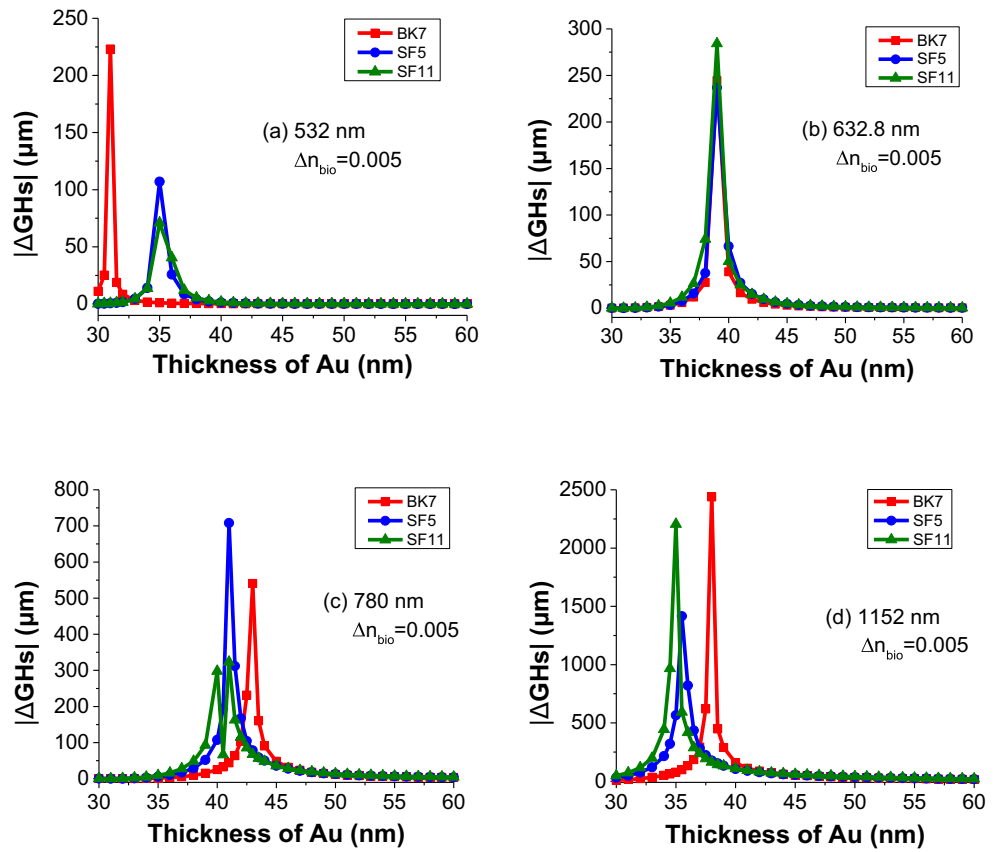


**Fig. 6** The modular change in differential GH shift  $|\Delta\text{GHs}|$  with the number of graphene layers at several thicknesses of gold film and with the combination of wavelength and prism of **a** 532 nm and SF11, **b** 632.8 nm and BK7, **c** 780 nm and BK7, and **d** 1152 nm and SF5 when the RI change of aqueous solution is  $\Delta n_{\text{bio}} = 0.005$

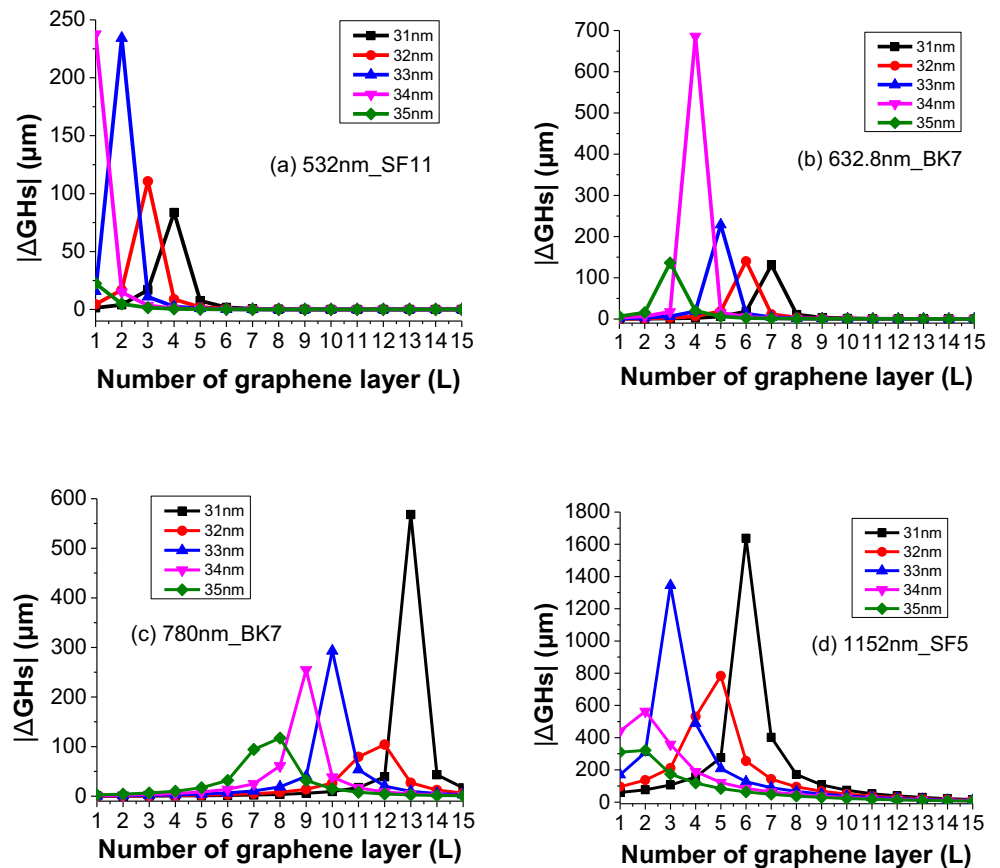


**Table 2** Optimal measured parameters at different fixed parameters showing the system characteristics based on Au/graphene/PtSe<sub>2</sub> sensing substrate ( $\Delta n_{\text{bio}} = 0.005$ )

Fixed parameters			Measured parameters									
$\lambda$ (nm)	Prism thickness (nm)	Gold thickness (nm)	Layer numbers of graphene ( $L$ )	PtSe <sub>2</sub> thickness (nm)	Resonance angle w/o biomolecules (°)	Resonance angle with biomolecules (°)	$ \Delta \text{GHs} $ ( $\mu\text{m}$ )	Sensitivity ( $\mu\text{m}/\text{RIU}$ )	FWTM w/o bio-molecules (°)	$R_{\text{min}}$ w/o bio-molecules	Sensitivity of the first model	Enhanced factor
532	BK7	31	0	2	78.89	79.81	223.13	44, 626	4.66	$4 \times 10^{-6}$	15, 608	2.86
632.8	BK7	34	4	2	74.70	75.44	685.97	137, 194	4.14	$1 \times 10^{-7}$	113, 817	1.21
780	BK7	43	0	2	68.03	68.60	540.63	108, 126	1.36	$1.3 \times 10^{-5}$	71, 295	1.52
780	BK7	34	3	4	70.83	71.44	1474.18	294, 836	3.61	$3 \times 10^{-7}$	71, 295	4.14
780	BK7	31	13	2	71.53	72.14	567.89	113, 578	4.67	$2 \times 10^{-6}$	71, 295	1.59
780	SF11	34	6	2	53.85	54.18	654.90	130, 980	1.92	$5 \times 10^{-6}$	82, 514	1.59
780	SF11	37	3	2	53.28	53.60	640.59	128, 118	1.33	$1.6 \times 10^{-5}$	82, 514	1.55
780	SF11	33	7	2	54.06	54.39	745.55	149, 110	2.14	$3 \times 10^{-6}$	82, 514	1.81
780	SF11	34	0	4	54.11	54.45	663.98	132, 796	2.04	$1 \times 10^{-5}$	82, 514	1.61
1152	BK7	38	0	2	64.08	64.55	2438.67	487, 734	0.77	$1.3 \times 10^{-5}$	339, 421	1.44
1152	BK7	34	0	6	65.58	66.08	3122.91	624, 582	1.59	$3 \times 10^{-6}$	339, 421	1.84
1152	SF5	34	2	2	55.49	55.83	2521.77	504, 354	1.38	$2.2 \times 10^{-5}$	153, 232	3.29
1152	SF5	33	3	2	55.59	55.93	1345.00	269, 000	0.83	$4.5 \times 10^{-5}$	153, 232	1.76
1152	SF5	31	6	2	55.87	56.21	1638.19	327, 638	1.06	$1.9 \times 10^{-5}$	153, 232	2.14
1152	SF5	32	3	4	56.07	56.41	1133.71	226, 742	1.06	$8 \times 10^{-6}$	153, 232	1.48
1152	SF11	35	0	2	50.76	51.04	2204.85	440, 970	0.64	$4.1 \times 10^{-5}$	223, 936	1.97
1152	SF11	34	1	2	50.84	51.13	2843.43	568, 686	0.60	$2.3 \times 10^{-5}$	223, 936	2.54
1152	SF11	30	5	4	51.61	51.90	2284.16	456, 832	1.11	$2 \times 10^{-6}$	223, 936	2.04

**Table 3** Sensitivity comparison of SPR-based sensors

SPR interrogation system	Enhancement strategy	Sensitivity	Reference
Angular change	Au/Si/graphene	135 (°/RIU)	[29]
Phase change	Au/Si/MoSe <sub>2</sub>	1.1 × 10 <sup>7</sup> (°/RIU)	[30]
GH shift change	Slab waveguide	6 × 10 <sup>2</sup> (μm)	[31]
GH shift change	Au/graphene/PtSe <sub>2</sub>	6.25 × 10 <sup>5</sup> (μm/RIU)	Current work

with the wavelength leading to less energy loss due to electronic damping. This means the detection accuracy improves during this process. Other SPR curves with the same parameters but different thicknesses of PtSe<sub>2</sub> can be seen in Fig. S2. The corresponding GH shift peaks, shown in Fig. 4b, become narrow and high due to the sharpest phase change at SPR angles, which lead to the largest GH shift at the excitation wavelength of 1152 nm when coupled by BK7 prism with the gold and PtSe<sub>2</sub> thicknesses being 34 nm and 6 nm, respectively.

The biomolecules in analyte solutions with various concentrations adsorb on the sensing layer, making a local change of RI near the sensing interface and changing the SPR resonance condition since it has a close relationship with the refractive index of dielectric medium. Specifically, after coating 2D material on the gold film, the optimum gold thickness for the first model corresponding to the largest differential GH shift between *p*- and *s*-polarized lights will differ with the incident wavelength. Figure 5 presents the modular change in differential GH shift |ΔGHs| with respect to the gold layer thickness under different excitation conditions with the RI change of Δ*n*<sub>bio</sub> = 0.005. For BK7 prism, the variation pattern of the optimum thickness of gold film with the incident wavelength is the same as that of the first model. While for the other two prisms, the variation pattern with the wavelength changes from monotonous decline to first increase and then decrease because of the same variation pattern of the RI of PtSe<sub>2</sub> with the wavelength. On the whole, however, the optimum gold thickness for all situations, to obtain the largest differential GH shift, decreases because of extra energy loss introduced by the layer of PtSe<sub>2</sub> which can only be offset by reducing the thickness of gold thin film. The modular change in differential GH shift improves greatly for some cases indicating the unique effect of this 2D material for enhancing sensing performance. The modular change in differential GH shift |ΔGHs| with other thicknesses of PtSe<sub>2</sub> can be seen in Fig. S3.

For the third model, we investigate the associated effect of graphene on the improvement in the sensing of GH shift after adding several layers of graphene between gold and PtSe<sub>2</sub>. The number of layers of graphene *L* is chosen from 1 to 15. Figure 6 shows the results of the modular change in differential GH shift |ΔGHs| with respect to the layer numbers of graphene. Other variations with the layer numbers of graphene at different excitation wavelengths and prisms can be seen in

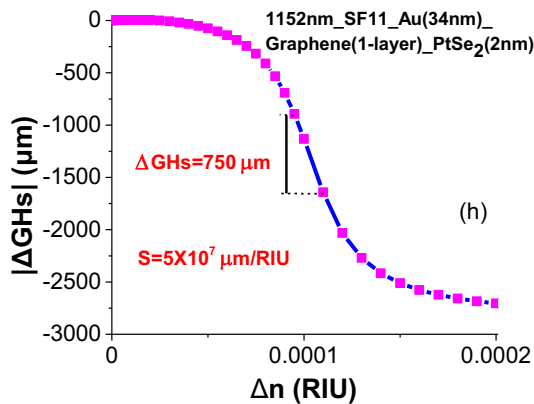
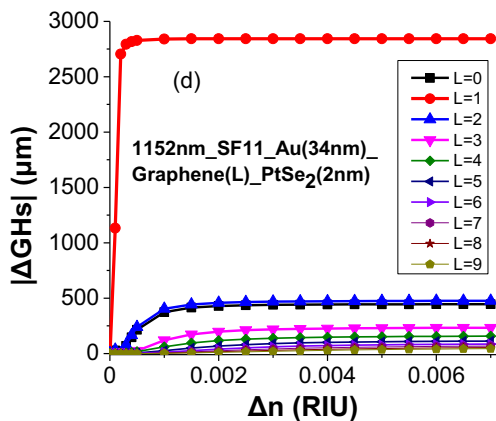
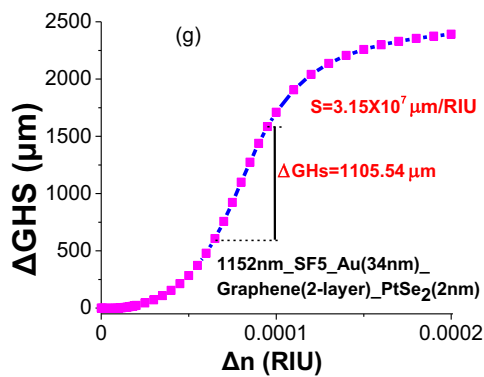
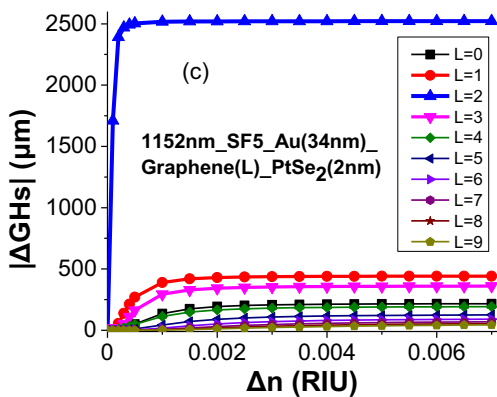
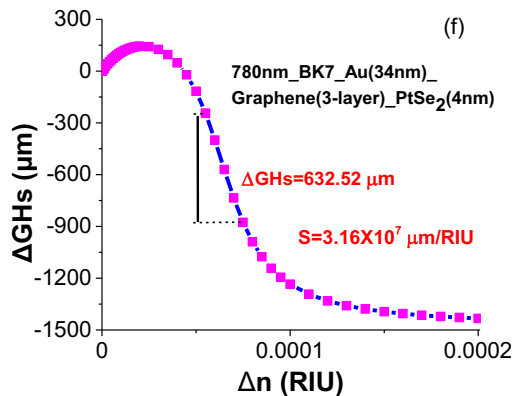
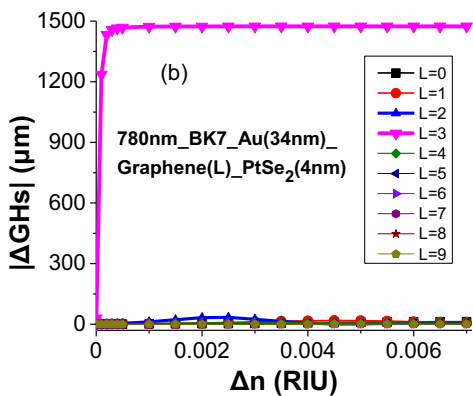
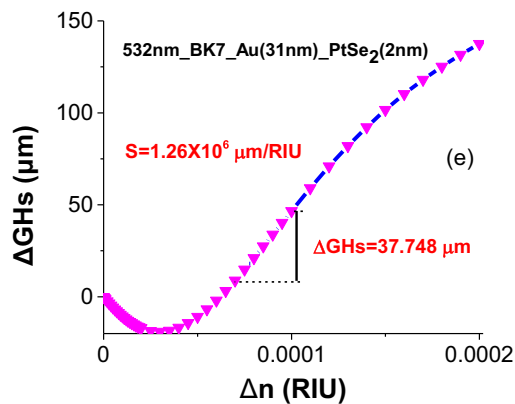
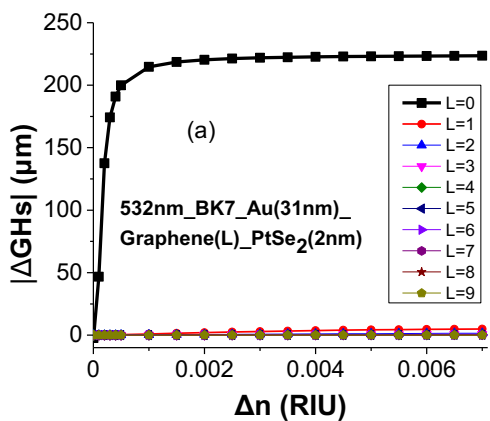
Fig. S4. We do not find a clearly unified law that states the direct connection between the layer numbers of graphene and the gold thickness for achieving the best sensing signal. But it is quite clear that the GH shift increases largely with certain layers of graphene; this may attribute to its excellent optoelectronic properties and precise adjustable thickness. In addition, in order to get the largest possible |ΔGHs|, it is really not necessary to have a high thickness of gold or a large value of *L*, because the higher thickness of gold or graphene will cause more energy absorption. For a given parameter set, there is only one optimum number of graphene layer to balance the signal enhancement and absorption loss leading to the sharpest phase change.

Table 2 lists some optimal configurations that we achieved on considering the parameters—the excitation wavelength, the different types of prisms, gold thickness, the layer numbers of graphene, and the PtSe<sub>2</sub> thickness—and tuning them to achieve the largest modular change in differential GH shift |ΔGHs| and the smallest width of SPR curve (FWTM ≤ 5°). We assume an RI change of Δ*n*<sub>bio</sub> = 0.005 for the sensing layer.

Compared with the changes in resonance angle which are no more than 1°, the modular changes in differential GH shift are always larger than the results of angle interrogation. That is to say, it is much easier to detect the signal of GH shift change. Moreover, the largest GH shift change always corresponds to the nearly zero reflectivity *R*<sub>min</sub>, which is so small for every configuration under different excitation wavelengths that the efficiency of energy transfers to SPR is very high. The FWTM of the SPR curve increases rapidly with decreasing wavelength, the layer numbers of graphene and the PtSe<sub>2</sub> thickness, from about 1° to almost 5°, mainly due to the RI change tendencies of prisms and gold. Enhanced factor indicates large improved sensing performance of these configurations in comparison with the sensitivity of conventional sensors only with gold as the sensing substrate. A suitable combination of all the layered materials can yield a more efficient sensing system.

**Fig. 7** a–d Modular change in differential GH shift |ΔGHs| with respect to the RI change of aqueous solutions under different layer numbers of graphene. The used wavelengths and prisms are selected from the optimum values shown in Table 2. e–h ΔGHs curves for the configurations obtained from a–d with optimal graphene layers with respect to tiny changes in RI of analyte solutions





We also compare several SPR-based sensors using different sensing signals, as seen in Table 3. Although the GH shift sensitivity slightly below that of phase interrogation, it is far more than that of angular interrogation and waveguide assistant GH shift sensor, particularly with the characteristics of easy measurement and low cost. Based on the above discussion, there are four optimized sensing configurations that should be further investigated their sensing performance. The four configurations are (i) 2 nm of PtSe<sub>2</sub> structured on 31 nm of Au and coupled by BK7 prism at a wavelength of 532 nm, (ii) 4 nm of PtSe<sub>2</sub> with triple-layer graphene structured on 34 nm of Au and coupled by BK7 prism at a wavelength of 780 nm, (iii) 2 nm of PtSe<sub>2</sub> with bilayer graphene structured on 34 nm of Au and coupled by SF5 prism at a wavelength of 1152 nm, and (iv) 2 nm of PtSe<sub>2</sub> with monolayer graphene structured on 34 nm of Au and coupled by SF11 prism at a wavelength of 1152 nm.

Figure 7 a–d show the modular change in differential GH shift  $|\Delta\text{GHs}|$  with the change in RI of the analyte solutions from 0 to 0.007 RI unit (RIU) for different numbers of graphene layer for the four selected configurations. The  $|\Delta\text{GHs}|$  changes significantly for the optimum configurations than for the non-optimum ones, and they quickly saturate with a tiny increase of RI. For some cases, the  $\Delta\text{GHs}$  changes from positive to negative or vice versa presenting the local small dip or peak of the curve. It should further refine the change of RI with tiny steps and keep the sign of  $\Delta\text{GHs}$  for better understanding the sensing performance.

The tiny step of refractive index change is first set to  $1 \times 10^{-6}$  when  $\Delta n_{\text{bio}}$  increases from 0 to 0.00002, and then increased to  $5 \times 10^{-6}$ . Figure 7 e–h show the differential GH shift change  $\Delta\text{GHs}$  with respect to the tiny RI change for the four optimum configurations. All these curves have different variation tendencies, but all of them are nonlinear. Moreover, the data difference can be as high as twenty times indicating that not all of the optimum configurations are suitable for detecting the GH shift signal at very small concentration changes of analyte solutions. There may be a blank detection region where the curve of change in differential GH shift crosses the zero point, and whose width is

determined by the values on both sides. For example, for the configuration of 2 nm of PtSe<sub>2</sub> structured on 31 nm of Au and coupled by BK7 prism at a wavelength of 532 nm, it is hard to detect the GH shift signal when the RI change of the solution is within the range of 0.000055 RIU to 0.000065 RIU. However, we can still find a linear change region in every curve. The corresponding sensitivities are also shown in the figures. The GH shift sensitivity for tiny changes in RI manifests 10- to 100-fold enhancement than that for large changes in RI, showing more enhanced sensing performance for a small RI change, and more sensitive to detect minute molecules in the vicinity of sensing interface. Considering the precision of position sensing detector (Thorlabs, PDP90A) used in our laboratory, a lateral shift more than 2  $\mu\text{m}$  can be effectively detected. Therefore, the detection limit for each optimum sensing configuration has a slight difference except one having much lower detection limit, as shown in Table 4. Additionally, compared with the conventional sensor, the detection limit of the optimum sensing configurations can be reduced by 2 orders of magnitude, and the sensitivity can significantly improve by 3 orders of magnitude.

At last, one point should be noticed is that the GH shift peaks for some cases are extremely high and narrow, which are actually determined by the definition of GH shift under stationary phase theory. The differential of phase singularity with the excitation of SPR may cause an error to some extent, which is the limitation of this method. Even though the drastic phase change around the resonance angle of SPR makes the GH shift value looked not so reasonable (the continuous phase change with the number of graphene layer is shown in Fig. S5, which also indicates indirectly the influence of graphene layers on the GH shift), the change tendencies of the GH shift with respect to the incident angle and the thicknesses of graphene and PtSe<sub>2</sub> as well as the conditions for achieving the peaks of GH shift are correct and still valuable to guide the related experiment. In addition, the electric distributions of surface fields in the vicinity of sensing interface, as seen in Fig. S6, indicate that the evanescent field can effectively extend in the aqueous solution, especially for long wavelengths.

**Table 4** Comparison of the detection limit of GH shift sensing performance of the conventional and four proposed sensing configurations

$\lambda$ (nm)	Prism	Enhanced configuration	Detection limit $\Delta n$ (RIU)	$\Delta\text{GHs}$ ( $\mu\text{m}$ )	Sensitivity ( $\mu\text{m}/\text{RIU}$ )
780	SF5	Au (44nm)	$5 \times 10^{-5}$	2.45	$4.9 \times 10^4$
532	BK7	Au(31nm)_PtSe <sub>2</sub> (2nm)	$2 \times 10^{-6}$	2.42	$1.2 \times 10^6$
780	BK7	Au(34nm)_Graphene(3-layer)_PtSe <sub>2</sub> (4nm)	$5 \times 10^{-7}$	7.55	$1.51 \times 10^7$
1152	SF5	Au(34nm)_Graphene(2-layer)_PtSe <sub>2</sub> (2nm)	$3 \times 10^{-6}$	2.16	$7.2 \times 10^5$
1152	SF11	Au(34nm)_Graphene(1-layer)_PtSe <sub>2</sub> (2nm)	$2 \times 10^{-6}$	2.53	$1.27 \times 10^6$

## Conclusion

In summary, we have employed two-dimensional materials of graphene and PtSe<sub>2</sub> to form plasmonic sensing substrates to achieve enhanced GH shift detection sensitivity. The intriguing optical absorption rate of graphene and PtSe<sub>2</sub> and fine adjustment thicknesses allow the achievement of ultralow light reflectivity at the SPR resonance angle. This minimum reflectivity leads to the abrupt phase change at the special incident angle and makes the lateral GH shift extremely sensitive to the RI change caused by adsorbing biomolecules which is contained in the aqueous solutions near the sensing interface. This adsorption is achieved by van der Waals force or ion force rather than functionalized layers. We have systematically optimized all parameters—the gold thickness and PtSe<sub>2</sub> thickness, the layer numbers of graphene, the excitation wavelengths, and the types of coupling prisms. And we proposed four optimum configurations to improve the overall sensing performance at wavelengths ranging from visible light to near-infrared band. Among them, the configuration of 780-nm wavelength light incident on a 4-nm thickness of PtSe<sub>2</sub> and triple-layer graphene structured on 34 nm of gold and coupled by BK7 prism yields the highest GH shift sensitivity enhancement, which is 4 times larger than that of conventional sensor. The detection limit of the RI change is as low as  $5 \times 10^{-7}$  RIU, which is reduced by 2 orders of magnitude compared with that of conventional gold sensor, and the corresponding sensitivity of biomolecules has a 1000-fold enhancement. A wide linear range of the tiny RI change from  $7 \times 10^{-5}$  to  $1 \times 10^{-4}$  with a large slope is obtained at the configuration of 2 nm thickness of PtSe<sub>2</sub> with bilayer graphene structured on 34 nm of gold and coupled by SF5 prism with incident light of 1152-nm wavelength.

**Funding Information** This work is supported by the National Natural Science Foundation of China (grant no. 11304070), the Singapore National Research Foundation and French National Research Agency grant NRF2017–ANR002 2DPS, China Scholarship Council.

## References

- Goos F, Hänchen H (1947) Ein neuer und fundamentaler versuch zur totalreflexion. *Ann Phys* 436:333–346
- Yuan L, Xiang L, Kong Y, Lu M, Lan Z, Zeng A, Wang Z (2012) Goos-Hänchen effect of spin electron beams in a parallel double  $\delta$ -barrier magnetic nanostructure. *Eur Phys J B* 85:8
- Chen X, Lu X, Wang Y, Li C (2011) Controllable Goos-Hänchen shifts and spin beam splitter for ballistic electrons in a parabolic quantum well under a uniform magnetic field. *Phys Rev B* 83:195409
- Sakata T, Togo H, Shimokawa F (2000) Reflection-type 2×2 optical waveguide switch using the Goos-Hänchen shift effect. *Appl Phys Lett* 76:2841
- Chen C, Lin W, Liao L, Lin Z, Chiang H, Leung P, Sijercic E, Tse WS (2007) Optical temperature sensing based on the Goos-Hänchen effect. *Appl Opt* 46:5347–5351
- Artmann K (1948) Berechnung der seitenversetzung des totalreflektierten strahles. *Ann Phys* 437:87–102
- Yonzon CR, Haynes CL, Zhang X, Walsh JT, Van Duyne RP (2004) A glucose biosensor based on surface-enhanced raman scattering: improved partition layer, temporal stability, reversibility, and resistance to serum protein interference. *Anal Chem* 76:78–85
- Wang Y, Li H, Cao Z, Yu T, Shen Q, He Y (2008) Oscillating wave sensor based on the Goos-Hänchen effect. *Appl Phys Lett* 92:061117
- Kong W, Wan Y, Li S, Zhao W, Zheng Z (2018) High-sensitivity Goos-Hänchen shift sensing based on Bloch surface wave. *Sens Actuators A Physical* 276:62–67
- Oh GY, Kim D, Choi YW (2009) The characterization of GH shifts of surface plasmon resonance in a waveguide using the FDTD method. *Opt Express* 17:20714–20720
- Hasib MHH, Nur JN, Rizal C, Shushama KN (2019) Improved transition metal dichalcogenides-based surface plasmon resonance biosensors. *Condens Matter* 4:49
- Yin X, Hesselink L (2006) Goos-Hänchen shift surface plasmon resonance sensor. *Appl Phys Lett* 89:261108
- Wan Y, Cheng M, Zheng Z, Liu K (2019) Polarization-modulated, Goos-Hänchen shift sensing for common mode drift suppression. *Sensors* 19:2088
- Periyanaounder D, Gnanasekar P, Varadhan P, He JH, Kulandaivel J (2018) High performance, self-powered photodetectors based on a graphene/silicon schottky junction diode. *J Mater Chem C* 6:9545–9551
- Liu B, Long M, Cai MQ, Yang J (2018) Two-dimensional van der Waals heterostructures constructed via perovskite (C<sub>4</sub>H<sub>9</sub>NH<sub>3</sub>)<sub>2</sub>XBr<sub>4</sub> and black phosphorus. *J Phys Chem Lett* 9:4822–4827
- Wang Y, Li L, Yao W, Song S, Sun JT, Pan J, Ren X, Li C, Okunishi E, Wang YQ, Wang E, Shao Y, Zhang YY, Yang H, Schwier EF, Iwasawa H, Shimada K, Taniguchi M, Cheng Z, Zhou S, Du S, Pennycook SJ, Pantelides ST, Gao HJ (2015) Monolayer PtSe<sub>2</sub>, a new semiconducting transition-metal-dichalcogenide, epitaxially grown by direct selenization of Pt. *Nano Lett* 15:4013–4018
- Guo GY, Liang WY (1986) The electronic structures of platinum dichalcogenides: PtS<sub>2</sub>, PtSe<sub>2</sub> and PtTe<sub>2</sub>. *J Phys C Solid State Phys* 19:995–1008
- Kandemir A, Akbali B, Kahraman Z, Badalov SV, Ozcan M, Iyikanat F, Sahin H (2018) Structural, electronic and phononic properties of PtSe<sub>2</sub>: from monolayer to bulk. *Semicond Sci Technol* 33:085002
- Xie J, Zhang D, Yan XQ, Ren M, Zhao X, Liu F et al (2019) Optical properties of chemical vapor deposition-grown PtSe<sub>2</sub> characterized by spectroscopic ellipsometry. *2D Mater* 6:035011
- Zhuang HL, Hennig RG (2013) Computational search for single-layer transition-metal dichalcogenide photocatalysts. *J Phys Chem C* 117:20440–20445
- Zhao Y, Qiao J, Yu Z, Yu P, Xu K, Lau SP, Zhou W, Liu Z, Wang X, Ji W (2017) High-electron-mobility and air-stable 2D layered PtSe<sub>2</sub> FETs. *Adv Mater* 29:1604230
- Yim C, Lee K, McEvoy N, O'Brien M, Riazimehr S, Berner NC, Cullen CP, Kotakoski J, Meyer JC, Lemme MC, Duesberg GS (2016) High-performance hybrid electronic devices from layered PtSe<sub>2</sub> films grown at low temperature. *ACS Nano* 10:9550–9558

23. Ciarrocchi A, Avsar A, Ovchinnikov D, Kis A (2018) Thickness-modulated metal-to-semiconductor transformation in a transition metal dichalcogenide. *Nat Commun* 9:919
24. Bruna M, Borini S (2009) Optical constants of graphene layers in the visible range. *Appl Phys Lett* 94:031901
25. Ouyang Q, Zeng S, Jiang L, Hong L, Xu G, Dinh XQ, Qian J, He S, Qu J, Coquet P, Yong KT (2016) Sensitivity enhancement of transition metal dichalcogenides/silicon nanostructure-based surface plasmon resonance biosensor. *Sci Rep* 6:28190
26. Refractive index database. Available at: <http://refractiveindex.info>
27. Johnson PB, Christy RW (1974) Optical constants of transition metals: Ti, V, Cr, Mn, Fe, Co, Ni, and Pd. *Phys Rev B* 9:5056–5070
28. Gupta BD, Sharma AK (2005) Sensitivity evaluation of a multi-layered surface plasmon resonance-based fiber optic sensor: a theoretical study. *Sensors Actuators B Chem* 107:40–46
29. Verma R, Gupta BD, Jha R (2011) Sensitivity enhancement of a surface plasmon resonance based biomolecules sensor using graphene and silicon layers. *Sensors Actuators B Chem* 160:623–631
30. Ouyang Q, Zeng S, Jiang L, Qu J, Dinh XQ, Qian J, He S, Coquet P, Yong KT (2017) Two-dimensional transition metal dichalcogenide enhanced phase-sensitive plasmonic biosensors: theoretical insight. *J Phys Chem C* 121:6282–6289
31. Taya SA, El-Farram EJ, El-Agez TM (2012) Goos-Hänchen shift as a probe in evanescent slab waveguide sensors. *Int J Electron Commun (AEU)* 66:204–210

**Publisher's Note** Springer Nature remains neutral with regard to jurisdictional claims in published maps and institutional affiliations.